physica status solidi b
www.pss-b.com
basic solid state physics

Graphene-sealed Si/SiN cavities for high-resolution *in situ* electron microscopy of nano-confined solutions

Haider Rasool[†,1,2], Gabriel Dunn[†,1,2], Aidin Fathalizadeh[1,2], and Alex Zettl[*,1,2,3]

[1] Department of Physics, University of California at Berkeley, Berkeley, CA 94720, USA
[2] Materials Sciences Division, Lawrence Berkeley National Laboratory, Berkeley, CA 94720, USA
[3] Kavli Energy NanoSciences Institute at the University of California, Berkeley and the Lawrence Berkeley National Laboratory, Berkeley, CA 94720, USA

[*] Corresponding author: e-mail **azettl@berkeley.edu**, Phone: +510 642 4939, Fax: +510 642 2685
[†] These authors contributed equally to this work.

We demonstrate new liquid cell architectures utilizing graphene-sealed Si or SiN cavities for *in situ* electron microscopy. While previous graphene liquid cell techniques have shown graphene to be an ideal sealing layer and electron-transparent viewing window, they trap irregular geometries of liquid with unknown sample volumes. Our new technique allows for a leak-proof confinement of liquids of precise volume in the tens of attoliter range while maintaining the benefits of graphene as a viewing window. The utility of this new cell architecture is demonstrated by imaging the dynamics of gold nanoparticles in three dimensions with atomic resolution under a transmission electron microscope.
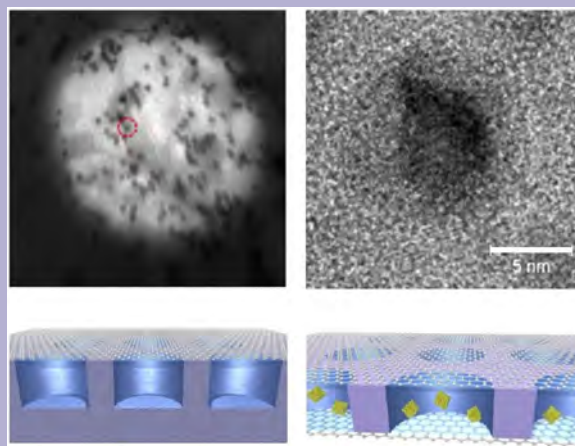
© 2016 WILEY-VCH Verlag GmbH & Co. KGaA, Weinheim

1 Introduction Understanding physical and chemical processes in liquid media is of fundamental interest to many branches of scientific research. Direct observation of chemical reactions with optical or electron microscopy provides critical insight into the details of reaction kinetics and dynamic physical processes. Of particular interest is the observation of liquids in confined spaces, where a confined space indicates a container size which is comparable to the size of the species of interest. For example, many native biological processes occur in confined vesicles comprised of a lipid bilayer container wall and facilitates the synthesis of peptides and hormones required to sustain cell function by enhancing the effective concentration of reacting species [1–4]. In synthetic chemistry, confined reaction environments formed from large organic molecules or porous solid state ceramics can change reaction pathways from those observed in bulk solution [5–9]. Recently, it has been shown that the effective equilibrium constant and reaction kinetics of a chemical reaction can depend on the container size for submicron cell dimensions [10–14].

While an extremely promising technique for the imaging of nanoscale processes in confined liquid samples, *in situ* transmission electron microscopy (TEM) poses a number of unique challenges. The high-vacuum environments of

electron microscopes require a liquid sample to be sealed within a leak-proof encapsulation. However, scattering from this encapsulating material, as well as the liquid sample itself, greatly limits the resolution, requiring both to be kept as thin as possible [15]. Liquid cells for *in situ* TEM were first formed using thin silicon nitride membranes as encapsulating layers which allowed for the sample thickness to be controlled with nanometer precision. However, the lateral dimensions of these cells remain on the millimeter scale and the thickness of nitride required for a stable cell causes enough scattering to significantly hinder their maximum achievable imaging resolution [16–19]. More recently, single atomic layer sheets of graphene have been used to seal liquids into random pockets. Being significantly thinner and having a smaller scattering cross-section due to its lower atomic mass, these graphene liquid cells allowed for the first atomic resolution *in situ* TEM imaging. While this method is capable of achieving exceptionally high resolution and is able to trap liquids effectively, the geometry of the trapped liquid cannot be controlled [20–23]. Without knowledge of the cell dimensions, analysis of the effect of nanoconfinement on diffusion dynamics and understanding of reaction kinetics is not possible.

In this work, we describe the fabrication of graphene capped liquid cells with well-defined dimensions and volumes in the tens of attoliter range. Pits or holes are formed in a silicon chip or a silicon nitride membrane using standard microfabrication techniques, where depth and cross-section can be precisely controlled. Graphene then serves as an ideal sealing material as it exhibits optical and electron transparency, is the thinnest and strongest possible viewing window, and has an ultra-strong adhesion to substrates with leak free containment, even in the demanding vacuum environment of a TEM. To demonstrate the utility of the developed cells, we image nanoparticle motion in liquid cells containing gold nanoparticles suspended in an aqueous buffer solution in TEM, and show that lattice plane resolution can be achieved [24].

2 Experimental Two different liquid cell geometries are made using graphene as the sealing material: a well-type cavity where pits are etched into a silicon chip and graphene is used to seal the top-side (Fig. 1(a) and (b)), and a channel-type cavity where ~500 nm diameter holes are etched into a suspended silicon nitride membrane and graphene is used to seal both sides (Fig. 1(c) and (d)). In both cases, the cavities are formed by focused ion beam (FIB) milling. The channel-type cavity is ideal for *in situ* TEM, as the total sample thickness is determined by the silicon nitride membrane, and the viewing path consists of only our sample and single atom thick layers of graphene.

A schematic of the assembly and sample encapsulation of the graphene-capped liquid cells is presented in Fig. 2. Graphene is first grown by chemical vapor deposition (CVD) on copper foil and one side is subsequently etched by oxygen plasma. A thin layer of 1% PMMA in anisole is spun onto the graphene side of the copper foil at a speed of 4000 rpm.
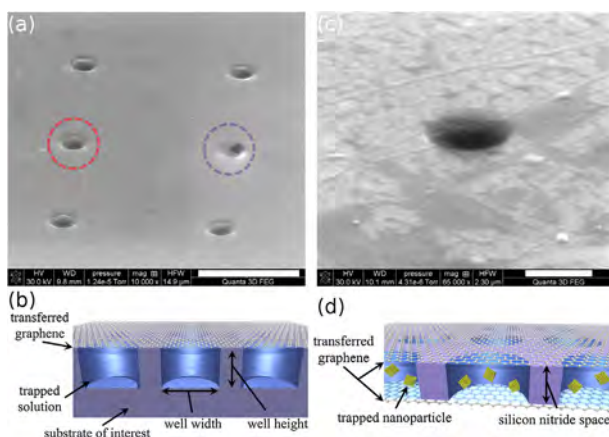
Figure 1 (a) SEM image of well-type liquid cell. Red circle shows intact graphene sealing layer with trapped liquid creating a bulge in the graphene film. Purple circle shows torn graphene sealing layer where no liquid is trapped. Scale bar, 5 μm. (b) Schematic of well-type liquid cell. (c) SEM image of channel-type liquid cell. The smaller hole size shows less bulging. Scale bar, 500 nm. (d) Schematic of channel-type liquid cell.

The copper foil is then placed in an etchant bath of sodium persulfate in water ($\sim$2 g mL^{-1}) to remove the copper substrate. The film is then transferred to a bath of 18 MΩ water. The film is again transferred to a bath of the desired trapping solution. A substrate with fabricated wells or holes is submerged into the bath and, in a single step, the receiving substrate is withdrawn from the solution pulling the graphene-PMMA film onto the surface and encapsulating the solution. Excess solution is removed from the surface with an absorbent. The sample is allowed to sit for 12–16 h to enhance graphene adhesion to the substrate before the PMMA is removed with acetone, and the sample is rinsed in isopropyl alcohol. In the case of the double-sided graphene sealed channel-type cells, the process is only slightly modified. The above steps are followed to apply the first graphene film to one of the sides of the silicon nitride after the water rinse and allowed to adhere to the substrate for 12–16 h. The graphene
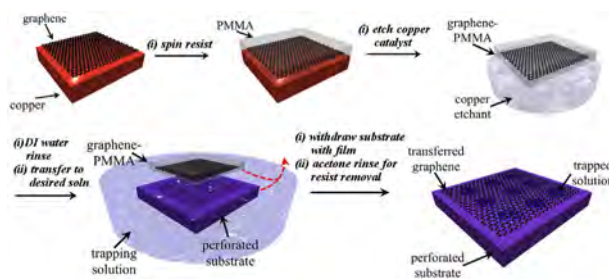
Figure 2 Graphene is CVD grown on a copper substrate, then coated in a thin layer of PMMA. The Cu substrate is etched away and the graphene/PMMA is transferred to a DI water rinse followed by the desired trapping solution. The sheet is then scooped out by the substrate with patterned cavities. For the capped-hole type cell, this procedure is repeated for both sides of the nitride membrane.

then provides the base of the well for the trapping of a desired solution in the above steps [25–26].

Sample encapsulation can be confirmed by SEM as is shown in Fig. 1a and c. Slight bulging can be seen by the shading on the graphene film under SEM and is due to the pressure differential between the trapped liquid and high-vacuum environment of the SEM, as well as the surface tension of the sample. When the graphene is torn or a hole is present, the liquid readily evaporates, and the remaining suspended graphene shows no bulging and the shading is then absent in the SEM scan. The encapsulation process typically results in an ∼80% yield of usable cells for well-type cells and a ∼40% yield for channel-type cells.

3 Results Using the described trapping method for a channel-type cell, we trap a solution of 10 nm gold nanoparticles (AuNPs) suspended in a phosphate buffer solution (PBS) to study the motion and interactions of the nanoparticles. PBS is a common solution used in biological experiments, which mimics the physiological conditions of a cell and is easily trapped using the above procedure. It is worth noting that were the acetone or isopropyl alcohol used to remove the PMMA from the graphene to have entered the cell, the buffer solution and the AuNPs would crash out of solution.

At lower dose rates, the cells appear stable and can be imaged indefinitely. However, upon exposure to a high intensity beam of illuminating electrons, the AuNPs begin to move within the cavity. The motion of one of the 10 nm AuNPs inside a 400 nm wide and 200 nm thick liquid cavity is highlighted in Fig. 3 using a JEOL 2010 TEM at an acceleration voltage of 80 kV. The particle begins with small movements with subsequent motion likely driven by the formation of expanding bubbles generated by hydrolysis of water under the intense electron beam irradiation. As the fluid current and oscillations evolve with time, the dynamic forces on the NP evolve as well, and generate large motions within the liquid chamber. After imaging at high intensity for upwards of 10 min, particle motion will cease and the cell will appear dry. This is likely due to a combination of tears in the graphene produced by electron beam damage or etching from radiolytic byproducts, and hydrolysis of the solution.

In addition to being able to image large-scale particle motion in the liquid cavity, it is possible to observe three dimensional (3D) particle motion at atomic resolution. Figure 4 shows a sequence of images taken with the Transmission Electron Aberration-Corrected Microscope 0.5 (TEAM 0.5) managed by the National Center for Electron Microscopy operated at 80 kV, where two particles move toward each other in the lateral plane while simultaneously changing their height within the cell. This change in height is evidenced by the change in the focus of the particles with time. In Fig. 4a, the two particles appear close to the focal condition of minimum contrast and as the particles move to the positions imaged in Fig. 4b, they develop Fresnel fringes indicating a change in height of the
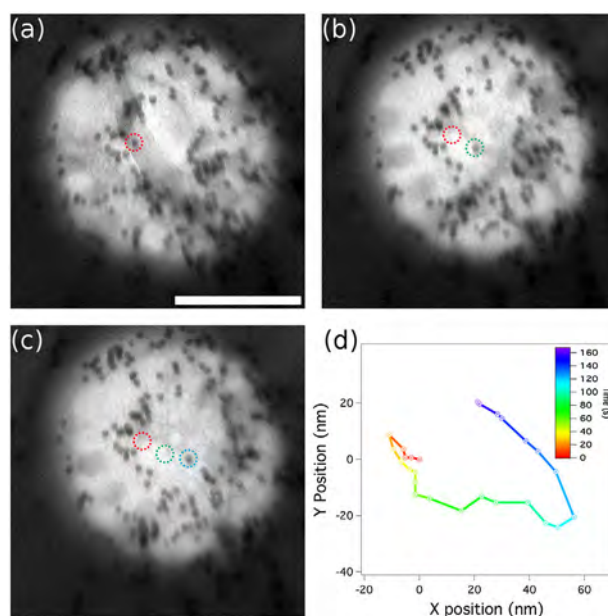
Figure 3 (a)–(c) TEM time series snapshots of Au-NPs trapped in a phosphate buffer solution. Bubbles formed by the hydrolysis of water under the electron beam drive the nanoparticle's movement. Scale bar, 250 nm. (d) Time series plot of the motion of the circled nanoparticle as it moves around the cell.

particle. The magnitude of this axial motion can be estimated from the transport of intensity equation as shown by Zhang and Oshima [27]. While observing 3D motion of the NPs in Fig. 4 and in Fig. 5, we observe clear atomic lattice fringes, allowing for further studies on particle
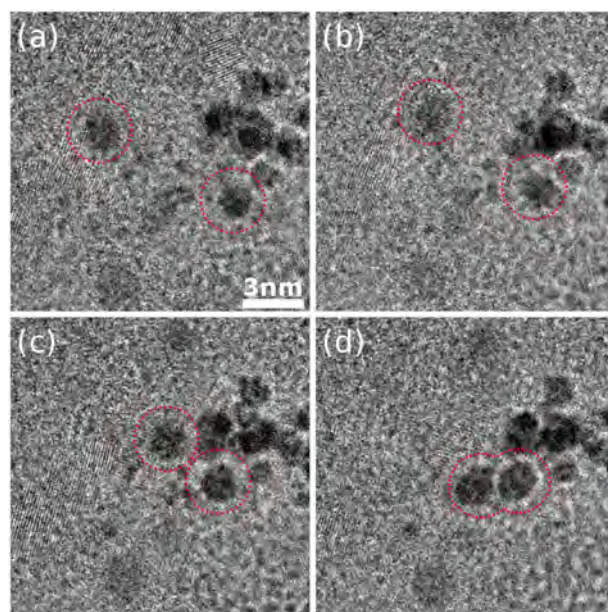
Figure 4 (a)–(d) TEM images of the axial motion of the two circled nanoparticles. While the other particles remain in the focal plane, these two fall out of focus and develop a ring around them, consistent with traveling out of the focal plane.
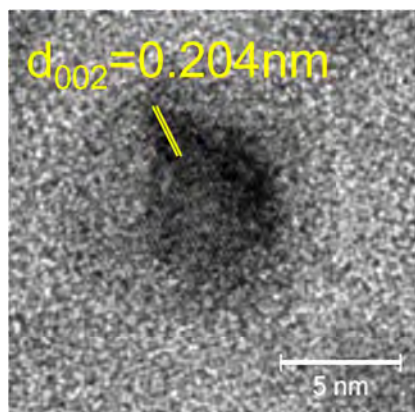
Figure 5 *In situ* TEM image of Au-NP in PBS demonstrates atomic-scale resolution. Lattice planes are clearly visible and spacing is consistent with the Au lattice constant.

rotations and surface reactions. With the ability to observe 3D motion with atomic resolution it is now possible to consider developing 3D particle tracking to observe a particle for an extended period of time and understand particle motion in confined space.

4 Conclusions In summary, we have developed a method to construct well defined liquid containers with graphene windows. These containers are remarkably robust and can remain intact in the harsh imaging environments required for electron microscopy. We demonstrate that gold nanoparticles suspended in a phosphate buffer solution, a common biological buffer, can easily be imaged using a TEM. The confined nanoparticles can be imaged on multiple length scales, down to 3D atomic resolution motion. These liquid cell containers have broad applications and may be used to study complex nanoparticle assemblies with more complex motions in a fully hydrated state.

References

[1] R. J. Ellis, Trends Biochem. Sci. **26**, 597–604 (2001).
[2] O. Medalia, I. Weber, A. S. Frangakis, D. Nicastro, G. Gerisch, and W. Baumeister, Science **298**, 1209–1213 (2002).
[3] R. J. Ellis and A. P. Minton, Nature **425**, 27–28 (2003).
[4] D. Hall and A. P. Minton, Biochim. Biophys. Acta **1649**, 127–139 (2003).
[5] T. Sawada, M. Yoshizawa, S. Sato, and M. Fujita, Nature Chem. **1**, 53–56 (2009).
[6] D. M. Vriezema, M. C. Aragonés, J. A. A. W. Elemans, J. J. L. M. Cornelissen, A. E. Rowan, and R. J. M. Nolte, Chem. Rev. **105**, 1445–1489 (2005).
[7] Y. D. Tretyakov, A. V. Lukashin, and A. A. Eliseev, Russ. Chem. Rev. **73**, 899–921 (2004).
[8] J. Fan, W. Shui, P. Yang, X. Wang, Y. Xu, H. Wang, X. Chen, and D. Zhao, Chem. Eur. J. **11**(5391), 5396 (2005).
[9] A. Kuschel and S. Polarz, J. Am. Chem. Soc. **132**(18), 6558–6565 (2010).
[10] A. Thomas, S. Polarz, and M. Antonietti, J. Phys. Chem. B **107**(21), 5081–5087 (2003).
[11] M. Polak and L. Rubinovich, Nano Lett. **8**, 3543–3547 (2008).
[12] J. S. Kim and A. Yethiraj, Biophys. J. **96**(4), 1333–1340 (2009).
[13] M. J. Shon and A. E. Cohen, J. Am. Chem. Soc. **134**, 14618–14623 (2012).
[14] L. Rubinovich and M. Polak, Nano Lett. **13**, 2247–2251 (2013).
[15] N. De Jonge and F. M. Ross, Nature Nanotechnol. **6**, 695 (2011).
[16] M. J. Williamson, R. M. Tromp, P. M. Vereecken, R. Hull, and F. M. Ross, Nature Mater. **2**, 532–536 (2003).
[17] H. Zheng, R. K. Smith, Y. Jun, C. Kisielowski, U. Dahmen, and A. P. Alivisatos, Science **324**, 1309–1312 (2009).
[18] H. Liao, S. Whitelam, and H. Zheng, Science **336**, 1011 (2012).
[19] H. Liao, D. Zherebetskyy, H. Xin, C. Czarnik, P. Ercius, H. Elmlund, M. Pan, L. Wang, and H. Zheng, Science **345**, 916 (2014).
[20] J. M. Yuk, J. Park, P. Ercius, K. Kim, D. J. Hellebusch, M. F. Crommie, J. Y. Lee, A. Zettl, and A. P. Alivisatos, Science **336**, 61–64 (2012).
[21] J. Park, H. Elmlund, P. Ercius, J. M. Yuk, D. T. Limmer, Q. Chen, K. Kim, S. H. Han, D. A. Weitz, A. Zettl, and A. P. Alivisatos, Science **349**, 290–294 (2015).
[22] Q. Chen, J. M. Smith, J. Park, K. Kim, D. Ho, H. I. Rasool A. Zettl, and A. P. Alivisatos, Nano Lett. **13**(9), 4556–4561 (2013).
[23] J. M. Yuk, Q. Zhou, J. Chang, P. Ercius, A. P. Alivisatos, and A. Zettl, ACS Nano **10**, 88–92 (2015).
[24] J. Lu, Z. Aabdin, N. D. Loh, D. Bhattacharya, and U. Mirsaidov, Nano Lett. **14**, 2111–2115 (2014).
[25] X. Li, W. Cai, J. An, S. Kim, J. Nah, D. Yang, R. Piner, A. Velemakanni, I. Jung, E. Tutuc, S. K. Banerjee, L. Colombo, and R. S. Ruoff, Science **324**(5932), 1312–1314 (2009).
[26] W. Regan, N. Alem, B. Alemán, B. Geng, C. Girit, L. Maserati, F. Wang, M. Crommie, and A. Zettl, Appl. Phys. Lett. **96**, 113102 (2010).
[27] X. Zhang and Y. Oshima, Microscopy **64**(6), 395–400 (2015).